

Preparation of a Modified Micro-arc Oxidation Coating Using Al_2O_3 Particles on Ti6Al4V

Hong Li^{1*} and Jin Zhang²¹Guangdong Institute of New Materials, National Engineering Laboratory for Modern Materials Surface Engineering Technology, The Key Lab of Guangdong for Modern Surface Engineering Technology, Guangzhou 510650, PR China²Beijing Key Laboratory for Corrosion, Erosion and Surface Technology, University of Science and Technology Beijing, Beijing 100083, PR China

Abstract

A micro-arc oxidation coating on Ti6Al4V alloy was modified by addition of micro- Al_2O_3 particles to a sodium phosphate solution. The coating structure and phase were characterized by scanning electron microscopy and X-ray diffraction, and the oxidation resistance and thermal shock properties of the coating were investigated. Results showed that a coating denser than the original coating was produced. This new coating was composed of Al_2TiO_5 and TiO_2 . The oxidation resistance and thermal shock property of the coating improved with addition of Al_2O_3 particles to the electrolyte relative to the sample prepared without the particles in the electrolyte. Moving Al_2O_3 particles were adsorbed on the coating surface and penetrated through it. As a result, the phase structure and properties of the original coating were modified.

Keywords: Ti6Al4V; Micro-arc oxidation; Al_2O_3 particle; Oxidation resistance; Thermal shock property

Introduction

Titanium alloys are widely used in the aerospace and biomedical industries for their low density, high relative strength, and good corrosion resistance. However, these alloys exhibit poor tribological behavior and anti-oxidation resistance at high temperatures. Micro-arc oxidation (MAO) is a new surface modification technique widely investigated in recent years and employed to produce different kinds of coatings on Ti alloys with improved properties [1-8]. Basically, the composition of the MAO coating depends on the substrate (Mg, Al, or Ti alloy) and the electrolyte. For example, TiO_2 , Al_2O_3 , and SiO_2 coatings are generally prepared in phosphate [9], aluminate [10], and silicate [9] solutions, respectively. Other composite coatings in mixing solutions [11] are used on titanium alloys. The porous structure of the MAO coating is generated from the micro-arc property of the approach [12]. The in situ growth behavior of the MAO coating underlies its good adhesion to the substrate [13]. Favorable thermal resistance of the MAO coating has also been reported [14,15]. The MAO coating prepared in Na_2SiO_3 - Na_2CO_3 - NaOH on Ti6Al4V exhibited good anti-oxidation properties at 500°C for 200 h [14]. The coating prepared in sodium phosphate with $\text{Co}(\text{CH}_3\text{COO})_2$ addition on Ti6Al4V exhibited thermal shock resistance at 500°C for 40 cycles [15]. Also, the functional coatings prepared on Ti alloys using MAO technology attracted recent attention. The black coating, first produced in the 1980s by the original anode oxidation technique or the cathode plasma oxidation method [16,17], is obtained in mixed electrolyte [18]. Overall, the coating properties are mostly dependent on the electrolyte employed. In this paper, a MAO coating much denser than usual was prepared on Ti6Al4V alloy by addition of Al_2O_3 particles to sodium phosphate solution. The coating's effects on anti-oxidation at 700°C and thermal shock at 850°C were studied.

Experiment Methods

Coating preparation

The substrate material used in this investigation was Ti6Al4V titanium alloy, with a chemical composition (wt.%) of 6.3 Al, 4.2 V, 0.15 O, 0.11 Fe, 0.03 C, 0.02 N, 0.001 H, and Ti balance. Specimens measuring 20 mm × 15 mm × 2 mm were ground using 60#, 120#,

400#, 600#, 1000#, and 1500# grit silicon carbide papers. The specimens were then cleaned using distilled water and acetone and subsequently air dried. For MAO treatment, a pulse power supply was employed, and the Ti6Al4V plate was used as the anode electrode. A graphite plate was used as the cathode in the electrolytic cell. The electrolyte was composed of an aqueous solution containing 0.3 mol/L sodium phosphate solution and 6 g/L Al_2O_3 particles dispersed by a magnetic stirrer. During MAO treatment, the temperature of the electrolyte was maintained below 45°C. The applied parameters are shown in Table 1. MAO coatings prepared in sodium phosphate solution without Al_2O_3 particles were used as a basis for comparison. After treatment, the obtained samples were washed with distilled water and dried at room temperature. The samples were then designated as TMPAI (Al_2O_3 particles within electrolyte) and TMP (without Al_2O_3 particles in the electrolyte).

Characterization of the coating

The Al_2O_3 particle sizes were measured by a laser diffraction particle size analyzer (LMS-30). The current was noted and the growth kinetics curves were plotted. The roughness of the samples was measured by a roughness gauge (TR200, Time Group Inc., China). The thicknesses of the coatings were measured by an eddy-current coating thickness gauge at three different points, and measurements were performed thrice

Voltage/V	Pulse frequency/Hz	Duty ratio/%	Time/min
500	2000	60	10

Table 1: Parameters for MAO coating preparation.

*Corresponding author: Hong Li, Guangdong Institute of New Materials, National Engineering Laboratory for Modern Materials Surface Engineering Technology, The Key Lab of Guangdong for Modern Surface Engineering Technology, Guangzhou 510650, PR China, Tel: 86-20 37238071; E-mail: leehong Aaron@163.com

Received October 18, 2017; Accepted November 02, 2017; Published November 12, 2017

Citation: Li H, Zhang J (2017) Preparation of a Modified Micro-arc Oxidation Coating Using Al_2O_3 Particles on Ti6Al4V. J Material Sci Eng 6: 400. doi: 10.4172/2169-0022.1000400

Copyright: © 2017 Li H, et al. This is an open-access article distributed under the terms of the Creative Commons Attribution License, which permits unrestricted use, distribution, and reproduction in any medium, provided the original author and source are credited.

(TT260, Time Group, Bei Jing). The phase component of the samples was analyzed by X-ray diffraction (XRD; Cu K α radiation, DMAX-RB, scanning in the range of $2\theta=10^{\circ}$ - 80° , 0.02° /step, 40 kV, and 150 mA). Scanning electron microscopy (SEM; FEI Quanta250 Environmental scanning electron microscope) was conducted to observe the coating morphology.

Coating properties

A thermal high-temperature cyclic oxidation test was performed in a kryptol heater furnace at 700°C in air for 100 h. A ceramic crucible was used to hold the sample and pre-heated to a constant weight. The Ti6Al4V substrate and the coating sample, both previously weighed, were oxidized at 700°C for 10 h. All of the specimens were then brought out, cooled naturally in air to room temperature, and then weighed again. Afterward, the samples were returned to the furnace for the next cycle. The test was performed for 10 thermal cycles, and the kinetic curve of each weight variant per unit area versus time was plotted.

A thermal shock test was conducted to evaluate the thermal shock property of the coating and the bond strength between the coating and substrate. The coated sample was placed inside a furnace at 850°C for 10 min. The specimen was then immediately removed, immersed in cool water, and returned to the furnace for the subsequent cycle. The thermal shock test was repeated for 30 cycles. The surface morphology and thermal-control property of the coatings were observed.

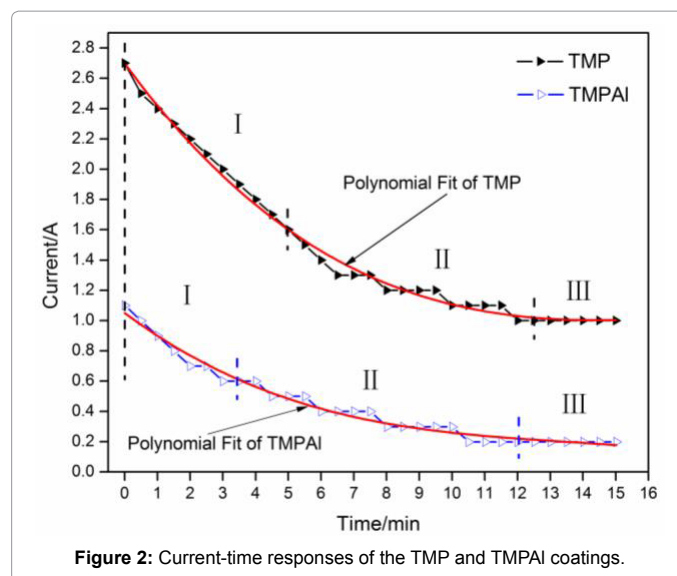
Result and Discussion

The particle size distribution of Al₂O₃

Figure 1 shows the particle size distribution of Al₂O₃ particles. The Al₂O₃ particles measure about 1 μ m and range in size between 0.3 and 3.6 μ m. The added Al₂O₃ particles were dispersed by a magnetic stirring apparatus located at the bottom of the container.

Current-time response

The current-time response of the TMP and TMPAI coatings are shown in Figure 2; three main regions [19] can be identified in both curves. The current-time curves initially declined linearly, gradually dipped, and then stabilized. By comparing the two curves, we noted that the current in the coat-forming process of TMPAI is lower than that of TMP and stabilizes at a very low value. Moving Al₂O₃ particles were adsorbed onto the coating surface and penetrated through it. The particles were then surrounded by the melting ceramic because of the high temperature (4000 K) caused by micro-arc formation [20]. The



Al₂O₃ particles melted and recrystallized together, thereby increasing in volume. Many micro-arc pores were filled, and a denser coating was formed. A much lower current was also observed.

Weight gain, thickness, roughness, and hardness of the coatings

Figure 3a shows the weight gains and thicknesses of the coatings prepared in different electrolytes. The weight of TMPAI increased by about three times that of TMP because of addition of Al₂O₃ particles to the electrolyte. The absorbed Al₂O₃ particles are responsible for the weight gain. However, not much difference in thickness was observed between the coatings. The Al₂O₃ particles absorbed in the coating improved its compactness, thereby leaving the coating thickness unaffected. The weight gain and thickness data indicate that TMPAI is more compact than TMP.

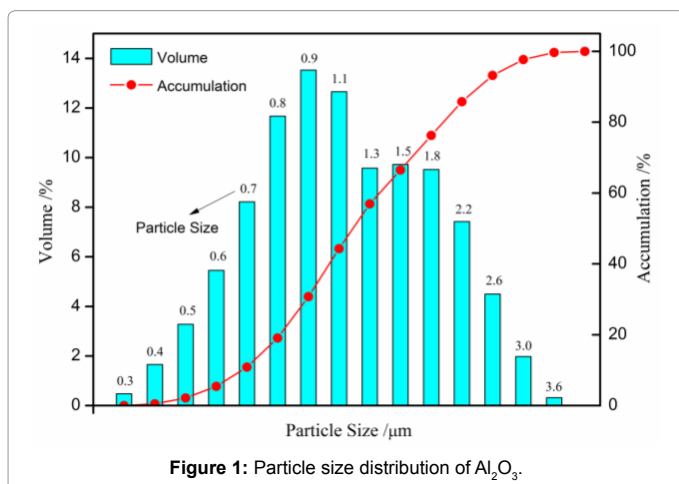
Figure 3b displays the hardness and roughness of the coatings. The hardness only slightly changes. As the hardness of a ceramic is usually affected by crystal texture, grain orientation, and grain size, no serious difference was noted between TMP and TMPAI, and both of the coatings exhibited similar crystal textures and grain sizes. However, the roughness of the TMPAI coating decreases from 4.5 μ m to 3.5 μ m with respect to that of TMP. Thus, coating roughness can be decreased by Al₂O₃ particle addition to the electrolyte. Lower current of TMP at the stable period causes the sparse and small micro-arc reaction that leads to the gentle structure of the corresponding coating. Hence, the roughness of TMP slightly decreased.

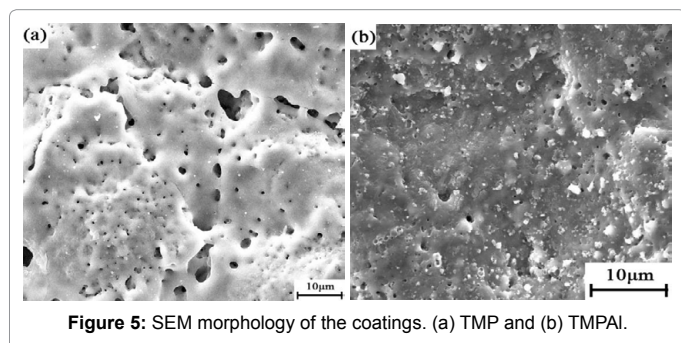
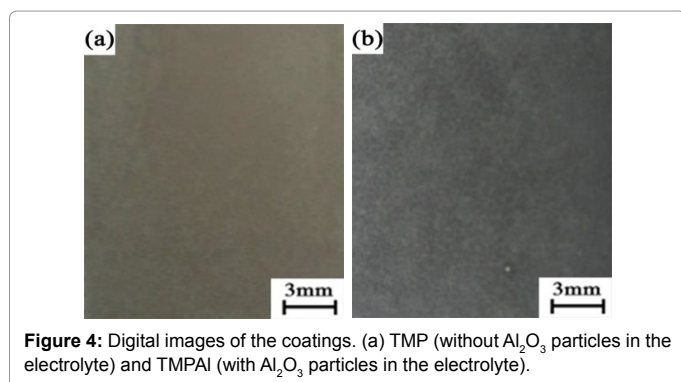
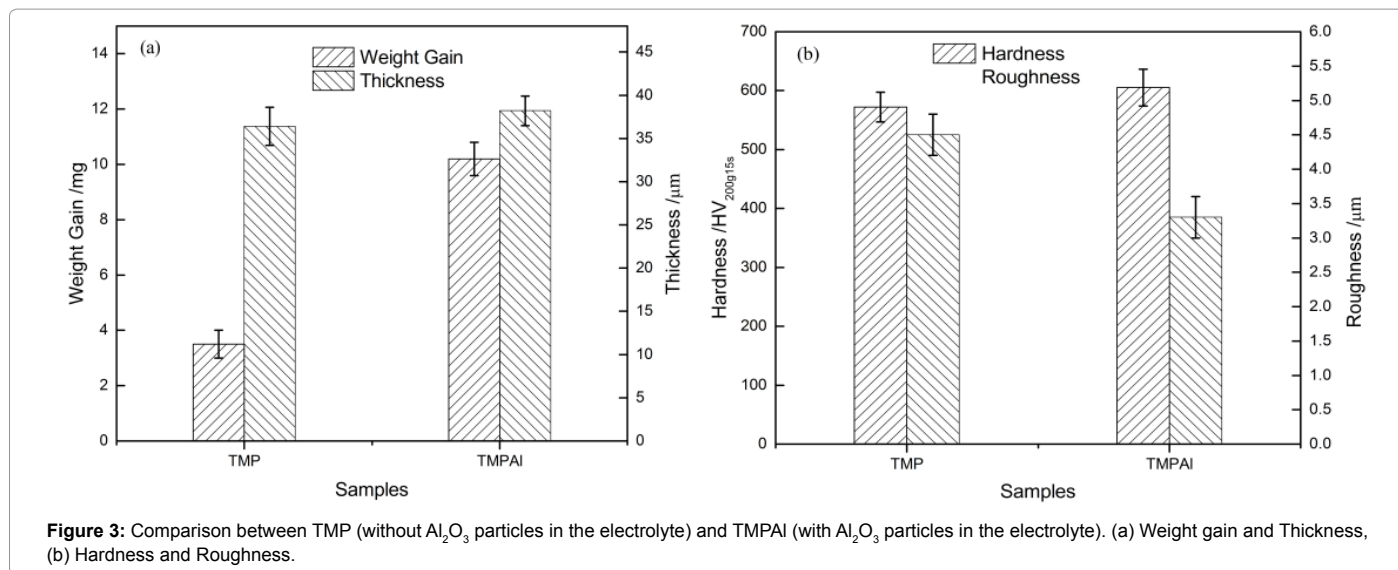
Macroscopic surface morphologies of the coatings

Figure 4 displays the digital images of the coatings prepared with and without Al₂O₃ particles in the phosphate solution. Both coatings exhibited uniform macroscopic surface morphology. However, the colors of TMP and TMPAI are light gray and iron gray, respectively.

Microcosmic surface morphologies of the coatings

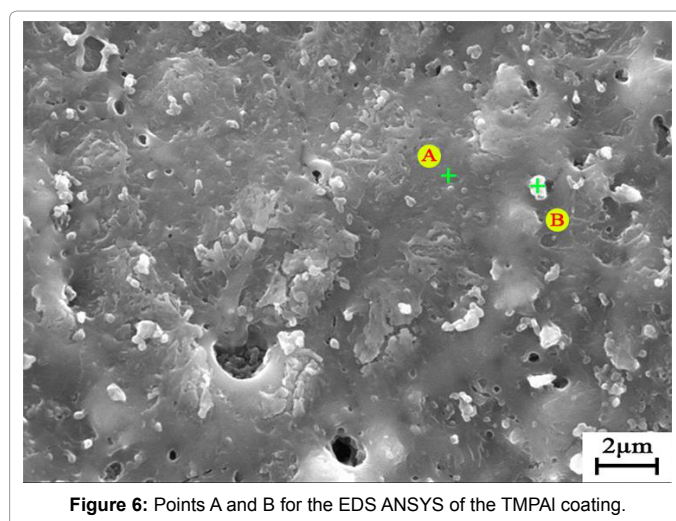
The microscopic surface morphologies of the coatings are depicted in Figure 5. Many micron-sized pores [21,22] generated by the micro-arc reaction are observed on the surface of TMP, whereas a few pores exist on the TMPAI surface. The micro-arc occurs at applied voltages above the breakdown voltage of the gas layer enshrouding the substrate.





The generation of a micro-arc depends on the applied voltage and the gas layer formed by the anodic oxidation reaction. The moving Al_2O_3 particles constantly affect the gas layer; hence, these particles do not produce sufficient plasma to create a micro-arc. Pores were fewer and smaller on the surface of the TMPAI coating than on the TMP coating. Meanwhile, the coating density and conductivity affects the process of anodic oxidation. The density of TMPAI was better than that of TMP, judging from the difference in weight gain and thickness (Figure 2). Throughout the experiment, the current of TMPAI was lower than that of TMP. Hence, less micro-arc was generated on the surface of TMPAI leading to fewer pores than that of TMP.

Two key points on the surface of the TMPAI coating were marked



in Figure 6 for energy dispersive spectroscopy (EDS) ANSYS. Many microparticles appeared attached and covering the coating surface. Table 2 shows the EDS results of point A and B. A dense area was noted at around point A, mainly composing of O, Al, Ti, and a small amount of P. P originates from the electrolyte after firing at high temperatures caused by micro-arc [23]. Al mostly comes from the added Al_2O_3 particles in the electrolyte. O is contributed by the Al_2O_3 particles and the oxidation of Ti. The determined levels of O, Al, and Ti conform to the composition of Al_2O_3 and TiO_2 . Hence, the composition of point A resembles those of Al_2O_3 , TiO_2 , and the combination of Al_2O_3 and TiO_2 .

Point B, which appears to correspond to an added Al_2O_3 particle, appears to be composed of O, Al, Ti, and some P. Compared with that in point A, the content of Ti in point B is apparently low. By contrast, the relative amounts of O, Al and Ti also resembles the composition of Al_2O_3 and TiO_2 . And, the main composition is Al_2O_3 , so the point B can be concluded to the Al_2O_3 particle.

Section morphologies of the coatings

Figure 7 reveals the section morphologies of the coatings. The existence of both porous and dense layers considered to be typical of

Position	Content (at%)			
	O	Al	Ti	P
A	62.55	18.73	17.82	0.90
B	58.94	34.78	5.50	0.78

Table 2: Elemental composition of the TMPAl coating at points A and B.

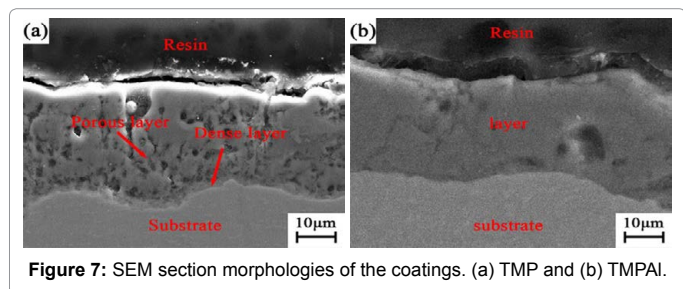


Figure 7: SEM section morphologies of the coatings. (a) TMP and (b) TMPAl.

the MAO coating structure [24] was noted in TMP, whereas a uniform layer was observed in TMPAl.

In MAO processes, temperatures generated by the micro-arc reaction can reach 4000 K [20]. When this event occurs, the surrounding material (mainly a TiO₂ ceramic) is melted and sputtered. As the micro-arc disappears and the electrolyte cools, the melted material begins to solidify to form volcano-like pores. The micro-arc reaction is also produced inside the coating because of the high voltage, thereby producing internal pores. With the increase in reaction time, the quantity and intensity of the micro-arc on the surface decreases. The oxygen penetrates the coating through a discharge channel to reach the surface of the Ti substrate and form titanium dioxide, which constitutes the dense layer.

The moving Al₂O₃ particle is adsorbed on the sample surface and penetrates into the melting material [25]. The melting points of titanium dioxide and aluminum oxide both approach 2100 K; thus, penetrating Al₂O₃ fuses and solidifies with the melting TiO₂. Two theories may explain the dense-layer formation with Al₂O₃ addition. The first conjecture proposes that the volume increases with the particle addition and aids help in filling the pores. The other hypothesis suggests that the decrease in current with Al₂O₃ addition to electrolyte under the same parameters reduces the quantity and intensity of the micro-arc. As free pores form in the entire process, less pores form inside the coating, and less micro-arc discharge is generated internally.

The elemental distribution across the TMPAl coating cross section is depicted in Figure 8. Similar to the EDS results in Table 2, a small amount of P was found in the cross section. The elemental composition of the TMPAl coating on the surface to a thickness of 10 µm constitutes Ti, O, and Al in stable values. From 10 µm to nearly 20 µm deeper into the coating, Ti content gradually increases to the Ti content in the Ti6Al4V substrate. By contrast, the Al and O contents gradually decrease to the contents of Al and O in Ti6Al4V, respectively.

Coating phases

Figure 9 shows the XRD patterns of TMP, TMPAl, and their oxidized counterparts. The main phase of the coating prepared in sodium phosphate solution without Al₂O₃ particles correspond to metastable anatase TiO₂ at low temperature, thermodynamically stable rutile TiO₂ at almost all temperatures, and Ti (Figure 9d). These results are similar to that previously reported [26]. During the MAO process, the anode Ti6Al4V is oxidized to form anatase TiO₂, part of which transforms to rutile TiO₂ under the high temperatures produced by

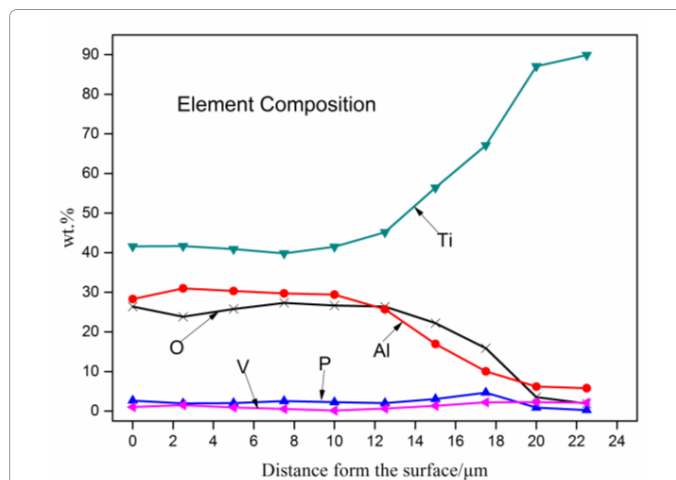


Figure 8: Elemental distribution along the cross section of the TMPAl coating.

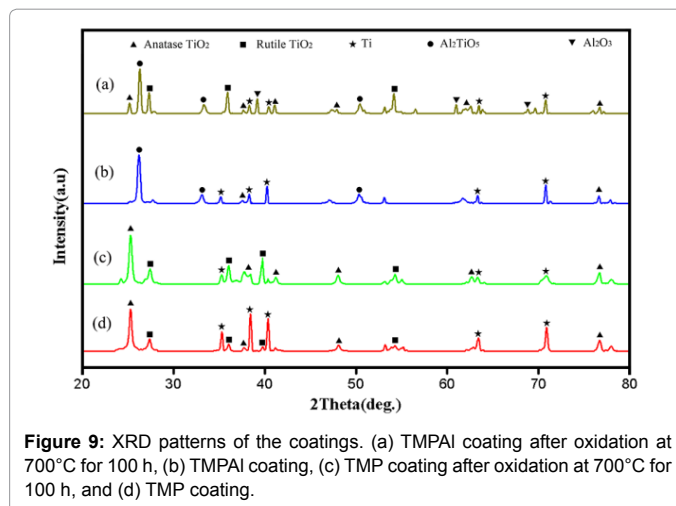


Figure 9: XRD patterns of the coatings. (a) TMPAl coating after oxidation at 700°C for 100 h, (b) TMPAl coating, (c) TMP coating after oxidation at 700°C for 100 h, and (d) TMP coating.

the micro-arc discharge. Furthermore, the discharge channel promotes the migration of Ti in the substrate to the coating. With increasing coating thickness, the previously formed coating becomes calcined and sputtered, allowing the transfer of some of the Ti in the substrate to the coating. After oxidation at 700°C for 100 h, Ti oxidizes to titanium dioxide (Figure 9c). As the transformation temperature of anatase TiO₂ to rutile TiO₂ is reached at 600°C, much more rutile TiO₂ is found.

The main phase of the coating prepared in sodium phosphate solution with Al₂O₃ particles constitute Al₂TiO₅, Ti, and some anatase TiO₂ (Figure 9b). The reported temperature of the following reaction [27] was 1553 K. In the formation process, the Al₂O₃ particle is absorbed into the melting TiO₂ to form Al₂TiO₅. The presence of Ti is caused by the permeation in high-voltage conditions and sputtering by the micro-arc. Similar to that in TMP, the Ti in the TMPAl coating becomes oxidized into anatase TiO₂ and rutile TiO₂ (Figure 9a). Moreover, Al₂TiO₅ is partially decomposed to TiO₂ and Al₂O₃ as shown in the equation below:



High-temperature oxidation of samples

Figure 10 shows the curves of weight gain after oxidation for the coating samples and substrate versus time under isothermal cyclic

oxidation at 700°C for 100 h. After oxidation, the color of Ti6Al4V drastically changes; the brown oxide coating is generated and obtains massive spalling with time. The TMP transforms from light grey to light yellow, whereas the TMPAI changed only slightly. No spalling pieces were found on both TMP and TMPAI after oxidation. Notably, the oxidation kinetics curve of Ti6Al4V follows parabolic kinetics before 30 h because the oxide coating does not spall from the substrate. Then, the curve assumes linear kinetics, as the oxide coating begins to spall gradually. TMP and TMPAI showed good surface morphologies; no piece spalled from the substrate. The weight gains of TMP and TMPAI are 0.78 mg/cm² and 0.60 mg/cm², respectively, illustrating that the coating samples of TMP and TMPAI can both provide good oxidation resistance for Ti6Al4V at 700°C for 100 h. The weight gains of TMP and TMPAI mainly caused by the oxidation of Ti were observed in the coatings. The content of Ti in TMP is substantially greater than that in TMPAI as shown by the contrast in XRD patterns (Figure 7b and 7d). Hence, the weight gain of TMP is much higher than that of TMPAI. The good oxidation resistance properties of TMP and TMPAI are attributed to the phase and coating structure. The main phases of TMP and TMPAI comprise TiO₂, Al₂O₃, and Al₂TiO₅, having low oxygen diffusion coefficients. The structure of TMP contains both porous and dense layers. Although many pores exist in the porous layer, these pores are insufficient, and thus, no channels are available for oxygen to reach the substrate. By contrast, TMPAI possess fewer pores, and consequently, oxygen is much more difficult to pass through the TMPAI coating.

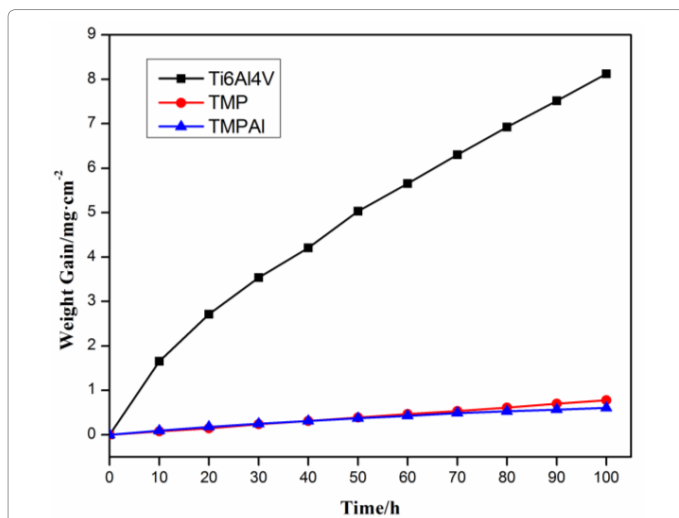


Figure 10: The oxidation kinetics curves of the samples at 700°C for 100 h. (TMP: without particle in solution, TMPAI: Al₂O₃ particle within solution).

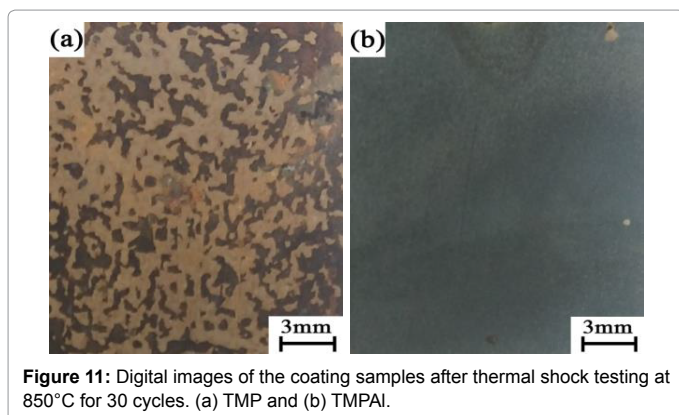


Figure 11: Digital images of the coating samples after thermal shock testing at 850°C for 30 cycles. (a) TMP and (b) TMPAI.

Sample	n	k _p	D	Equation
Ti6Al4V	1.4875	0.2161	1.5562E ⁻⁰⁰⁴	$\Delta W^{1.4875}=0.2161t$
TMP	1.0162	0.008253	5.7177E ⁻⁰⁰⁴	$\Delta W^{1.0162}=0.0082t$
TMPAI	1.9525	0.00752	0.0048	$\Delta W^{1.9525}=0.0075t$

Table 3: Fitting oxidation kinetic equations of the Ti6Al4V substrate and TMP and TMPAI coating samples.

According to the Wagner's theory of oxidation, oxidation weight gain and oxidation time can be expressed by the following relationship:

$$\Delta W^n = k_p t \quad (2)$$

where n is the reaction index, k_p is the reaction constant (function of temperature), ΔW is the weight gain, and t is the oxidation time. The method of linear regression was adopted to fit the curve and calculate the reaction index and reaction constant. The fitting equation is show in Table 3.

From the value of n in Table 3, continuous oxidation is used to describe the oxidation of the Ti6Al4V substrate as the oxidation film spalls off with time. Linear oxidation occurs on the TMP coating, whereas parabolic oxidation takes place on the TMPAI coating. Hence, the TMPAI coating can provide better anti-oxidation protection for Ti6Al4V than TMP in the long term.

Thermal shock of coatings

The surface macro-photograph of the coating samples is exhibited in Figure 11 after 30 times of thermal shock testing at 850°C. A large area of TMP peeled off, whereas some scattered oxidation points are displayed on the surface of TMPAI. These points indicate that the thermal shock resistance of the MAO coating prepared in sodium phosphate solution can be improved by the addition of appropriate Al₂O₃ particles in the electrolyte. The thermal shock property is used to describe the anti-thermal shock property of some coatings and the adhesion between the coating and substrate. The coating with high thermal expansion coefficient easily cracks with strong thermal stress. The thermal expansion coefficient disparity between the coating and substrate can cause the peeling from the substrate. The thermal expansion coefficient of TiO₂ and TiAl4V are 9 × 10⁻⁶ and 8.6 × 10⁻⁶ m/K, respectively, whereas that of Al₂TiO₅ is about 1.5 × 10⁻⁶ m/K [28]. The thermal shock test showed that the coating of TMP spalls more severely than TMPAI, which is attributed to the higher thermal expansion coefficient of TiO₂ than that of AlTiO5. Although a large gap in thermal expansion coefficient exists between Al₂TiO₅ and Ti6Al4V, the metallurgical bond between the coating and substrate can be protected from spalling. Moreover, during the coating preparation process, the current of TMP is higher than that of TMPAI. Stronger and more numerous micro-arc discharges are also created in the former than in the latter. Greater stress is generated in the process of repeated calcination, which magnifies the thermal stress and causes the cracking and spalling off of the coating.

Conclusion

Addition of Al₂O₃ particles to a sodium phosphate solution led to the preparation of a slightly porous coating by MAO on Ti6Al4V. The Al₂O₃ particles added to solution not only decreased the roughness but also improve the compactness of the coating. Al₂O₃ and Al₂TiO₅ phases combined in the slightly porous structure to provide good anti-oxidation effects at 700°C for 100 h. The low coefficient of thermal expansion of Al₂TiO₅ plays a crucial role in the anti-thermal-shock property of the coating at 850°C for 30 cycles.

Acknowledgments

This work was financially supported by the projects of science and technology foundation of Guangdong province (2016GDASPT-0206), key laboratory of Guangdong modern surface engineering technology (2017GDASCX-0111) and national engineering laboratory for modern materials surface engineering technology (2017GDASCX-0202).

References

1. Kim TS, Park YG, Wey MY (2003) Characterization of Ti-6Al-4V alloy modified by plasma carburizing process. *Materials Science and Engineering: A* 361: 275-280.
2. Tsunekawa S, Aoki Y, Habazaki H (2011) Two-step plasma electrolytic oxidation of Ti-15V-3Al-3Cr-3Sn for wear-resistant and adhesive coating. *Surface and Coatings Technology* 205: 4732-4740.
3. Song WH, Jun YK, Han Y, Hong SH (2004) Biomimetic apatite coatings on micro-arc oxidized titania. *Biomaterials* 25: 3341-3349.
4. Sun X, Jiang Z, Xin S, Yao Z (2005) Composition and mechanical properties of hard ceramic coating containing α -Al₂O₃ produced by microarc oxidation on Ti-6Al-4V alloy. *Thin Solid Films* 471: 194-199.
5. Curran JA, Clyne TW (2005) Thermo-physical properties of plasma electrolytic oxide coatings on aluminium. *Surface and Coatings Technology* 199: 168-176.
6. Tian J, Luo Z, Qi S, Sun X (2002) Structure and antiwear behavior of micro-arc oxidized coatings on aluminum alloy. *Surface and Coatings Technology* 154: 1-7.
7. Xue W, Wang C, Chen R, Deng Z (2002) Structure and properties characterization of ceramic coatings produced on Ti-6Al-4V alloy by microarc oxidation in aluminate solution. *Materials Letters* 52: 435-441.
8. Krishna LR, Poshal G, Jyothirmayi A, Sundararajan G (2015) Relative hardness and corrosion behavior of micro arc oxidation coatings deposited on binary and ternary magnesium alloys. *Materials & Design* 77: 6-14.
9. Yerokhin AL, Nie X, Leyland A, Matthews A (2000) Characterisation of oxide films produced by plasma electrolytic oxidation of a Ti-6Al-4V alloy. *Surface and Coatings Technology* 130: 195-206.
10. Wheeler JM, Collier CA, Paillard JM, Curran JA (2010). Evaluation of micromechanical behaviour of plasma electrolytic oxidation (PEO) coatings on Ti-6Al-4V. *Surface and Coatings Technology* 204: 3399-3409.
11. Habazaki H, Tsunekawa S, Tsuji E, Nakayama T (2012) Formation and characterization of wear-resistant PEO coatings formed on β -titanium alloy at different electrolyte temperatures. *Applied Surface Science* 259: 711-718.
12. Li XM, Han Y (2008) Mechanical properties of Ti (C0.7N0.3) film produced by plasma electrolytic carbonitriding of Ti6Al4V alloy. *Applied Surface Science* 254: 6350-6357.
13. Wang Y, Lei T, Jiang B, Guo L (2004) Growth, microstructure and mechanical properties of microarc oxidation coatings on titanium alloy in phosphate-containing solution. *Applied surface science* 233: 258-267.
14. Xu Y, Yao Z, Jia F, Wang Y, Jiang Z, et al. (2010) Preparation of PEO ceramic coating on Ti alloy and its high temperature oxidation resistance. *Current Applied Physics* 10: 698-702.
15. Tang H, Sun Q, Xin T, Yi C, Jiang Z, et al. (2012) Influence of Co (CH₃COO)₂ concentration on thermal emissivity of coatings formed on titanium alloy by micro-arc oxidation. *Current Applied Physics* 12: 284-290.
16. Hwang IJ, Shin KR, Lee JS, Ko YG, Shin DH (2012) Formation of black ceramic layer on aluminum alloy by plasma electrolytic oxidation in electrolyte containing Na₂WO₄. *Materials Transactions* 53: 559-564.
17. RVGP S TP (1997) A method for producing an optically black coatings on valve metals.
18. Yao Z, Hu B, Shen Q, Niu A, Jiang Z, et al. (2014) Preparation of black high absorbance and high emissivity thermal control coating on Ti alloy by plasma electrolytic oxidation. *Surface and Coatings Technology* 253: 166-170.
19. Li H, Sun Y, Zhang J (2015) Effect of ZrO₂ particle on the performance of micro-arc oxidation coatings on Ti6Al4V. *Applied Surface Science* 342: 183-190.
20. Hussein RO, Nie X, Northwood DO, Yerokhin A, Matthews A (2010) Spectroscopic study of electrolytic plasma and discharging behaviour during the plasma electrolytic oxidation (PEO) process. *Journal of Physics D: Applied Physics* 43: 105203.
21. Matykina E, Berkani A, Skeldon P, Thompson GE (2007) Real-time imaging of coating growth during plasma electrolytic oxidation of titanium. *Electrochimica Acta* 53: 1987-1994.
22. Wang Y, Jiang B, Lei T, Guo L (2004) Dependence of growth features of microarc oxidation coatings of titanium alloy on control modes of alternate pulse. *Materials Letters* 58: 1907-1911.
23. Robinson HJ, Markaki AE, Collier CA, Clyne TW (2011) Cell adhesion to plasma electrolytic oxidation (PEO) titania coatings, assessed using a centrifuging technique. *Journal of the mechanical behavior of biomedical materials* 4: 2103-2112.
24. Guangliang Y, Xianyi L, Yizhen B, Haifeng C, Zengsun J (2002) The effects of current density on the phase composition and microstructure properties of micro-arc oxidation coating. *Journal of Alloys and Compounds* 345: 196-200.
25. Li X, Luan BL (2012) Discovery of Al₂O₃ particles incorporation mechanism in plasma electrolytic oxidation of AM60B magnesium alloy. *Materials Letters* 86: 88-91.
26. Wang Y, Lei T, Jiang B, Guo L (2004) Growth, microstructure and mechanical properties of microarc oxidation coatings on titanium alloy in phosphate-containing solution. *Applied surface science* 233: 258-267.
27. Zhong Y, Shi L, Li M, He F, He X (2014) Characterization and thermal shock behavior of composite ceramic coating doped with ZrO₂ particles on TC4 by micro-arc oxidation. *Applied Surface Science* 311: 158-163.
28. Kim IJ, Supkwak H (2000) Thermal shock resistance and thermal expansion behaviour with composition and microstructure of Al₂TiO₅ ceramics. *Canadian metallurgical quarterly* 39: 387-396.